EUROPEAN ORGANIZATION FOR NUCLEAR RESEARCH

CERN–PPE/96-130

19 September 1996

Measurement of Event Shape and Inclusive Distributions at $\sqrt{s} = 130$ and 136 GeV

DELPHI Collaboration

Abstract

Inclusive charged particle and event shape distributions are measured using 321 hadronic events collected with the DELPHI experiment at LEP at effective centre of mass energies of 130 to 136 GeV. These distributions are presented and compared to data at lower energies, in particular to the precise Z data. Fragmentation models describe the observed changes of the distributions well. The energy dependence of the means of the event shape variables can also be described using second order QCD plus power terms. A method independent of fragmentation model corrections is used to determine α_s from the energy dependence of the mean thrust and heavy jet mass. It is measured to be:

$$\alpha_s(133 \text{ GeV}) = 0.116 \pm 0.007_{exp}{}^{+0.005}_{-0.004}{}_{theo}$$

from the high energy data.

(To be submitted to Zeit. für Physik C)

P.Abreu[21], W.Adam[50], T.Adye[37], I.Ajinenko[42], G.D.Alekseev[16], R.Alemany[49], P.P.Allport[22], S.Almehed[24], U.Amaldi[9], S.Amato[47], A.Andreazza[28], M.L.Andrieux[14], P.Antilogus[9], W-D.Apel[17], B.Åsman[44], J-E.Augustin[25], A.Augustinus[9], P.Baillon[9], P.Bambade[19], F.Barao[21], R.Barate[14], M.Barbi[47], G.Barbiellini[46], D.Y.Bardin[16], A.Baroncelli[40], O.Barring[24], J.A.Barrio[26], W.Bartl[50], M.J.Bates[37], M.Battaglia[15], M.Baubillier[23], J.Baudot[39], K-H.Becks[52], M.Begalli[6], P.Beilliere[8], Yu.Belokopytov[9,53], A.C.Benvenuti[5], M.Berggren[47], D.Bertini[25], D.Bertrand[2], M.Besancon[39], F.Bianchi[45], M.Bigi[45], M.S.Bilenky[16], P.Billoir[23], M-A.Bizouard[19], D.Bloch[10], M.Blume[52], T.Bolognese[39], M.Bonesini[28], W.Bonivento[28], P.S.L.Booth[22], C.Bosio[40], O.Botner[48], E.Boudinov[31], B.Bouquet[19], C.Bourdarios[9], T.J.V.Bowcock[22], M.Bozzo[13], P.Branchini[40], K.D.Brand[36], T.Brenke[52], R.A.Brenner[15], C.Bricman[2], R.C.A.Brown[9], P.Bruckman[18], J-M.Brunet[8], L.Bugge[33], T.Buran[33], T.Burgsmueller[52], P.Buschmann[52], A.Buys[9], S.Cabrera[49], M.Caccia[28], M.Calvi[28], A.J.Camacho Rozas[41], T.Camporesi[9], V.Canale[38], M.Canepa[13], K.Cankocak[44], F.Cao[2], F.Carena[9], L.Carroll[22], C.Caso[13], M.V.Castillo Gimenez[49], A.Cattai[9], F.R.Cavallo[5], V.Chabaud[9], M.Chapkin[42], Ph.Charpentier[9], L.Chaussard[25], P.Checchia[36], G.A.Chelkov[16], M.Chen[2], R.Chierici[45], P.Chliapnikov[42], P.Chochula[7], V.Chorowicz[9], J.Chudoba[30], V.Cindro[43], P.Collins[9], R.Contri[13], E.Cortina[49], G.Cosme[19], F.Cossutti[46], J-H.Cowell[22], H.B.Crawley[1], D.Crennell[37], G.Crosetti[13], J.Cuevas Maestro[34], S.Czellar[15], E.Dahl-Jensen[29], J.Dahm[52], B.Dalmagne[19], M.Dam[29], G.Damgaard[29], P.D.Dauncey[37], M.Davenport[9], W.Da Silva[23], C.Defoix[8], A.Deghorain[2], G.Della Ricca[46], P.Delpierre[27], N.Demaria[35], A.De Angelis[9], W.De Boer[17], S.De Brabandere[2], C.De Clercq[2], C.De La Vaissiere[23], B.De Lotto[46], A.De Min[36], L.De Paula[47], C.De Saint-Jean[39], H.Dijkstra[9], L.Di Ciaccio[38], A.Di Diodato[38], F.Djama[10], J.Dolbeau[8], M.Donszelmann[9], K.Doroba[51], M.Dracos[10], J.Drees[52], K.-A.Drees[52], M.Dris[32], J-D.Durand[25], D.Edsall[1], R.Ehret[17], G.Eigen[4], T.Ekelof[48], G.Ekspong[44], M.Elsing[52], J-P.Engel[10], B.Erzen[43], M.Espirito Santo[21], E.Falk[24], D.Fassouliotis[32], M.Feindt[9], A.Fenyuk[42], A.Ferrer[49], S.Fichet[23], T.A.Filippas[32], A.Firestone[1], P.-A.Fischer[10], H.Foeth[9], E.Fokitis[32], F.Fontanelli[13], F.Formenti[9], B.Franek[37], P.Frenkiel[8], D.C.Fries[17], A.G.Frodesen[4], R.Fruhwirth[50], F.Fulda-Quenzer[19], J.Fuster[49], A.Galloni[22], D.Gamba[45], M.Gandelman[47], C.Garcia[49], J.Garcia[41], C.Gaspar[9], U.Gasparini[36], Ph.Gavillet[9], E.N.Gazis[32], D.Gele[10], J-P.Gerber[10], L.Gerdyukov[42], R.Gokieli[51], B.Golob[43], G.Gopal[37], L.Gorn[1], M.Gorski[51], Yu.Gouz[45,53], V.Gracco[13], E.Graziani[40], C.Green[22], A.Grefrath[52], P.Gris[39], G.Grosdidier[19], K.Grzelak[51], S.Gumenyuk[28,53], P.Gunnarsson[44], M.Gunther[48], J.Guy[37], F.Hahn[9], S.Hahn[52], Z.Hajduk[18], A.Hallgren[48], K.Hamacher[52], F.J.Harris[35], V.Hedberg[24], R.Henriques[21], J.J.Hernandez[49], P.Herquet[2], H.Herr[9], T.L.Hessing[35], E.Higon[49], H.J.Hilke[9], T.S.Hill[1], S-O.Holmgren[44], P.J.Holt[35], D.Holthuizen[31], S.Hoorelbeke[2], M.Houlden[22], J.Hrubec[50], K.Huet[2], K.Hultqvist[44], J.N.Jackson[22], R.Jacobsson[44], P.Jalocha[18], R.Janik[7], Ch.Jarlskog[24], G.Jarlskog[24], P.Jarry[39], B.Jean-Marie[19], E.K.Johansson[44], L.Jonsson[24], P.Jonsson[24], C.Joram[9], P.Juillot[10], M.Kaiser[17], F.Kapusta[23], K.Karafasoulis[11], M.Karlsson[44], E.Karvelas[11], S.Katsanevas[3], E.C.Katsoufis[32], R.Keranen[4], Yu.Khokhlov[42], B.A.Khomenko[16], N.N.Khovanski[16], B.King[22], N.J.Kjaer[31], O.Klapp[52], H.Klein[9], A.Klovning[4], P.Kluit[31], B.Koene[31], P.Kokkinias[11], M.Koratzinos[9], K.Korcyl[18], V.Kostioukhine[42], C.Kourkoumelis[3], O.Kouznetsov[13,16], M.Krammer[50], C.Kreuter[17], I.Kronkvist[24], Z.Krumstein[16], W.Krupinski[18], P.Kubinec[7], W.Kucewicz[18], K.Kurvinen[15], C.Lacasta[49], I.Laktineh[25], J.W.Lamsa[1], L.Lanceri[46], D.W.Lane[1], P.Langefeld[52], V.Lapin[42], J-P.Laugier[39], R.Lauhakangas[15], G.Leder[50], F.Ledroit[14], V.Lefebure[2], C.K.Legan[1], R.Leitner[30], J.Lemonne[2], G.Lenzen[52], V.Lepeltier[19], T.Lesiak[18], J.Libby[35], D.Liko[50], R.Lindner[52], A.Lipniacka[44], I.Lippi[36], B.Loerstad[24], J.G.Loken[35], J.M.Lopez[41], D.Loukas[11], P.Lutz[39], L.Lyons[35], J.MacNaughton[50], G.Maehlum[17], J.R.Mahon[6], A.Maio[21], A.Malek[52], T.G.M.Malmgren[44], V.Malychev[16], F.Mandl[50], J.Marco[41], R.Marco[41], B.Marechal[47], M.Margoni[36], J-C.Marin[9], C.Mariotti[40], A.Markou[11], C.Martinez-Rivero[41], F.Martinez-Vidal[49], S.Marti i Garcia[22], J.Masik[30], F.Matorras[41], C.Matteuzzi[28], G.Matthiae[38], M.Mazzucato[36], M.Mc Cubbin[9], R.Mc Kay[1], R.Mc Nulty[22], J.Medbo[48], M.Merk[31], C.Meroni[28], S.Meyer[17], W.T.Meyer[1], M.Michelotto[36], E.Migliore[45], L.Mirabito[25], W.A.Mitaroff[50], U.Mjoernmark[24], T.Moa[44], R.Moeller[29], K.Moenig[9], M.R.Monge[13], P.Morettini[13], H.Mueller[17], K.Muenich[52], M.Mulders[31], L.M.Mundim[6], W.J.Murray[37], B.Muryn[18], G.Myatt[35], F.Naraghi[14], F.L.Navarria[5], S.Navas[49], K.Nawrocki[51], P.Negri[28], W.Neumann[52], N.Neumeister[50], R.Nicolaidou[3], B.S.Nielsen[29], M.Nieuwenhuizen[31], V.Nikolaenko[10], P.Niss[44], A.Nomerotski[36], A.Normand[35], W.Oberschulte-Beckmann[17], V.Obraztsov[42], A.G.Olshevski[16], A.Onofre[21], R.Orava[15], K.Osterberg[15], A.Ouraou[39], P.Paganini[19], M.Paganoni[9,28], P.Pages[10], R.Pain[23], H.Palka[18], Th.D.Papadopoulou[32], K.Papageorgiou[11], L.Pape[9], C.Parkes[35], F.Parodi[13], A.Passeri[40], M.Pegoraro[36], M.Pernicka[50], A.Perrotta[5], C.Petridou[46], A.Petrolini[13], M.Petrovyck[42], H.T.Phillips[37], G.Piana[13], F.Pierre[39], M.Pimenta[21], O.Podobrin[17], M.E.Pol[6], G.Polok[18], P.Poropat[46], V.Pozdniakov[16], P.Privitera[38], N.Pukhaeva[16], A.Pullia[28], D.Radojicic[35], S.Ragazzi[28], H.Rahmani[32], J.Rames[12], P.N.Ratoff[20], A.L.Read[33], M.Reale[52], P.Rebecchi[19], N.G.Redaelli[28], M.Regler[50], D.Reid[9], P.B.Renton[35], L.K.Resvanis[3], F.Richard[19], J.Richardson[22], J.Ridky[12], G.Rinaudo[45], I.Ripp[39], A.Romero[45], I.Roncagliolo[13], P.Ronchese[36], L.Roos[14], E.I.Rosenberg[1], E.Rosso[9], P.Roudeau[19], T.Rovelli[5], W.Ruckstuhl[31], V.Ruhlmann-Kleider[39], A.Ruiz[41], K.Rybicki[18], H.Saarikko[15], Y.Sacquin[39], A.Sadovsky[16], O.Sahr[14], G.Sajot[14], J.Salt[49], J.Sanchez[26], M.Sannino[13], M.Schimmelpfennig[17], H.Schneider[17], U.Schwickerath[17], M.A.E.Schyns[52], G.Sciolla[45], F.Scuri[46], P.Seager[20], Y.Sedykh[16], A.M.Segar[35], A.Seitz[17], R.Sekulin[37], L.Serbelloni[38], R.C.Shellard[6], P.Siegrist[39], R.Silvestre[39], S.Simonetti[39], F.Simonetto[36], A.N.Sisakian[16], B.Sitar[7], T.B.Skaali[33], G.Smadja[25], N.Smirnov[42], O.Smirnova[24], G.R.Smith[37], R.Sosnowski[51], D.Souza-Santos[6], T.Spassov[21], E.Spiriti[40], P.Sponholz[52], S.Squarcia[13], C.Stanescu[40], S.Stapnes[33], I.Stavitski[36], K.Stevenson[35], F.Stichelbaut[9], A.Stocchi[19], J.Strauss[50], R.Strub[10],

B.Stugu[4], M.Szczekowski[51], M.Szeptycka[51], T.Tabarelli[28], J.P.Tavernet[23], O.Tchikilev[42], J.Thomas[35], A.Tilquin[27], J.Timmermans[31], L.G.Tkatchev[16], T.Todorov[10], S.Todorova[10], D.Z.Toet[31], A.Tomaradze[2], B.Tome[21], A.Tonazzo[28], L.Tortora[40], G.Transtromer[24], D.Treille[9], W.Trischuk[9], G.Tristram[8], A.Trombini[19], C.Troncon[28], A.Tsirou[9], M-L.Turluer[39], I.A.Tyapkin[16], M.Tyndel[37], S.Tzamarias[22], B.Ueberschaer[52], O.Ullaland[9], V.Uvarov[42], G.Valenti[5], E.Vallazza[9], G.W.Van Apeldoorn[31], P.Van Dam[31], J.Van Eldik[31], A.Van Lysebetten[2], N.Vassilopoulos[35], G.Vegni[28], L.Ventura[36], W.Venus[37], F.Verbeure[2], M.Verlato[36], L.S.Vertogradov[16], D.Vilanova[39], P.Vincent[25], L.Vitale[46], E.Vlasov[42], A.S.Vodopyanov[16], V.Vrba[12], H.Wahlen[52], C.Walck[44], M.Weierstall[52], P.Weilhammer[9], C.Weiser[17], A.M.Wetherell[9], D.Wicke[52], J.H.Wickens[2], M.Wielers[17], G.R.Wilkinson[35], W.S.C.Williams[35], M.Winter[10], M.Witek[18], T.Wlodek[19], K.Woschnagg[48], K.Yip[35], O.Yushchenko[42], F.Zach[25], A.Zaitsev[42], A.Zalewska[9], P.Zalewski[51], D.Zavrtanik[43], E.Zevgolatakos[11], N.I.Zimin[16], M.Zito[39], D.Zontar[43], G.C.Zucchelli[44], G.Zumerle[36]

[1] Department of Physics and Astronomy, Iowa State University, Ames IA 50011-3160, USA
[2] Physics Department, Univ. Instelling Antwerpen, Universiteitsplein 1, B-2610 Wilrijk, Belgium
and IIHE, ULB-VUB, Pleinlaan 2, B-1050 Brussels, Belgium
and Faculté des Sciences, Univ. de l'Etat Mons, Av. Maistriau 19, B-7000 Mons, Belgium
[3] Physics Laboratory, University of Athens, Solonos Str. 104, GR-10680 Athens, Greece
[4] Department of Physics, University of Bergen, Allégaten 55, N-5007 Bergen, Norway
[5] Dipartimento di Fisica, Università di Bologna and INFN, Via Irnerio 46, I-40126 Bologna, Italy
[6] Centro Brasileiro de Pesquisas Físicas, rua Xavier Sigaud 150, RJ-22290 Rio de Janeiro, Brazil
and Depto. de Física, Pont. Univ. Católica, C.P. 38071 RJ-22453 Rio de Janeiro, Brazil
and Inst. de Física, Univ. Estadual do Rio de Janeiro, rua São Francisco Xavier 524, Rio de Janeiro, Brazil
[7] Comenius University, Faculty of Mathematics and Physics, Mlynska Dolina, SK-84215 Bratislava, Slovakia
[8] Collège de France, Lab. de Physique Corpusculaire, IN2P3-CNRS, F-75231 Paris Cedex 05, France
[9] CERN, CH-1211 Geneva 23, Switzerland
[10] Centre de Recherche Nucléaire, IN2P3 - CNRS/ULP - BP20, F-67037 Strasbourg Cedex, France
[11] Institute of Nuclear Physics, N.C.S.R. Demokritos, P.O. Box 60228, GR-15310 Athens, Greece
[12] FZU, Inst. of Physics of the C.A.S. High Energy Physics Division, Na Slovance 2, 180 40, Praha 8, Czech Republic
[13] Dipartimento di Fisica, Università di Genova and INFN, Via Dodecaneso 33, I-16146 Genova, Italy
[14] Institut des Sciences Nucléaires, IN2P3-CNRS, Université de Grenoble 1, F-38026 Grenoble Cedex, France
[15] Research Institute for High Energy Physics, SEFT, P.O. Box 9, FIN-00014 Helsinki, Finland
[16] Joint Institute for Nuclear Research, Dubna, Head Post Office, P.O. Box 79, 101 000 Moscow, Russian Federation
[17] Institut für Experimentelle Kernphysik, Universität Karlsruhe, Postfach 6980, D-76128 Karlsruhe, Germany
[18] Institute of Nuclear Physics and University of Mining and Metalurgy, Ul. Kawiory 26a, PL-30055 Krakow, Poland
[19] Université de Paris-Sud, Lab. de l'Accélérateur Linéaire, IN2P3-CNRS, Bât. 200, F-91405 Orsay Cedex, France
[20] School of Physics and Chemistry, University of Lancaster, Lancaster LA1 4YB, UK
[21] LIP, IST, FCUL - Av. Elias Garcia, 14-1^{o}, P-1000 Lisboa Codex, Portugal
[22] Department of Physics, University of Liverpool, P.O. Box 147, Liverpool L69 3BX, UK
[23] LPNHE, IN2P3-CNRS, Universités Paris VI et VII, Tour 33 (RdC), 4 place Jussieu, F-75252 Paris Cedex 05, France
[24] Department of Physics, University of Lund, Sölvegatan 14, S-22363 Lund, Sweden
[25] Université Claude Bernard de Lyon, IPNL, IN2P3-CNRS, F-69622 Villeurbanne Cedex, France
[26] Universidad Complutense, Avda. Complutense s/n, E-28040 Madrid, Spain
[27] Univ. d'Aix - Marseille II - CPP, IN2P3-CNRS, F-13288 Marseille Cedex 09, France
[28] Dipartimento di Fisica, Università di Milano and INFN, Via Celoria 16, I-20133 Milan, Italy
[29] Niels Bohr Institute, Blegdamsvej 17, DK-2100 Copenhagen 0, Denmark
[30] NC, Nuclear Centre of MFF, Charles University, Areal MFF, V Holesovickach 2, 180 00, Praha 8, Czech Republic
[31] NIKHEF, Postbus 41882, NL-1009 DB Amsterdam, The Netherlands
[32] National Technical University, Physics Department, Zografou Campus, GR-15773 Athens, Greece
[33] Physics Department, University of Oslo, Blindern, N-1000 Oslo 3, Norway
[34] Dpto. Fisica, Univ. Oviedo, C/P. Pérez Casas, S/N-33006 Oviedo, Spain
[35] Department of Physics, University of Oxford, Keble Road, Oxford OX1 3RH, UK
[36] Dipartimento di Fisica, Università di Padova and INFN, Via Marzolo 8, I-35131 Padua, Italy
[37] Rutherford Appleton Laboratory, Chilton, Didcot OX11 OQX, UK
[38] Dipartimento di Fisica, Università di Roma II and INFN, Tor Vergata, I-00173 Rome, Italy
[39] CEA, DAPNIA/Service de Physique des Particules, CE-Saclay, F-91191 Gif-sur-Yvette Cedex, France
[40] Istituto Superiore di Sanità, Ist. Naz. di Fisica Nucl. (INFN), Viale Regina Elena 299, I-00161 Rome, Italy
[41] Instituto de Fisica de Cantabria (CSIC-UC), Avda. los Castros, S/N-39006 Santander, Spain, (CICYT-AEN93-0832)
[42] Inst. for High Energy Physics, Serpukov P.O. Box 35, Protvino, (Moscow Region), Russian Federation
[43] J. Stefan Institute and Department of Physics, University of Ljubljana, Jamova 39, SI-61000 Ljubljana, Slovenia
[44] Fysikum, Stockholm University, Box 6730, S-113 85 Stockholm, Sweden
[45] Dipartimento di Fisica Sperimentale, Università di Torino and INFN, Via P. Giuria 1, I-10125 Turin, Italy
[46] Dipartimento di Fisica, Università di Trieste and INFN, Via A. Valerio 2, I-34127 Trieste, Italy
and Istituto di Fisica, Università di Udine, I-33100 Udine, Italy
[47] Univ. Federal do Rio de Janeiro, C.P. 68528 Cidade Univ., Ilha do Fundão BR-21945-970 Rio de Janeiro, Brazil
[48] Department of Radiation Sciences, University of Uppsala, P.O. Box 535, S-751 21 Uppsala, Sweden
[49] IFIC, Valencia-CSIC, and D.F.A.M.N., U. de Valencia, Avda. Dr. Moliner 50, E-46100 Burjassot (Valencia), Spain
[50] Institut für Hochenergiephysik, Österr. Akad. d. Wissensch., Nikolsdorfergasse 18, A-1050 Vienna, Austria
[51] Inst. Nuclear Studies and University of Warsaw, Ul. Hoza 69, PL-00681 Warsaw, Poland
[52] Fachbereich Physik, University of Wuppertal, Postfach 100 127, D-42097 Wuppertal, Germany
[53] On leave of absence from IHEP Serpukhov

1 Introduction

The running of the strong coupling constant α_s is a fundamental prediction of QCD, the theory of strong interactions. It is intimately connected to the properties of asymptotic freedom and confinement at large and small momentum transfer, respectively. Asymptotic freedom allows elementary strong interaction processes at large momentum transfer to be calculated reliably using perturbation theory. Confinement explains why only colour neutral objects are observed in nature.

Experimentally it is important to check the precise running of the strong coupling constant, which is predicted by the beta function defined by the renormalization group equation. The running of α_s is most easily accessible by studying the energy dependence of infrared-safe and collinear-safe event shape measures of the hadronic final state in e^+e^- annihilation. The α_s dependence of the average shape measure is predicted in second order QCD [1,2].

The hadronization process (the transformation of partons into observable hadrons) also has an impact on the energy dependence. However, it is expected to show an inverse power law behaviour in energy for many event shape variables, while the running of the strong coupling constant at parton level is logarithmic to first order.

The power law dependence is predicted by Monte Carlo fragmentation models and is also understood in terms of a simple tube model [3]. Even at the Z energy, these contributions are sizeable [4] and lead to significant uncertainties in the determination of α_s. In the last few years this topic has attracted much theoretical activity. Power corrections to event shapes have also been predicted due to infrared renormalons, and have been calculated assuming an infrared-regular behaviour of α_s at low energy scales [5–8].

This paper presents new experimental results from the high energy run of LEP at 130 GeV and 136 GeV in the autumn of 1995, with the aim of contributing to a better understanding of the energy dependence of event shape distributions. This may lead to a better description of the fragmentation process, which in turn contributes to a more precise study of the energy dependence of the strong coupling constant and finally to a more precise determination of α_s.

The paper is organized as follows. Section 2 discusses the detector, the data samples, and the cuts and corrections applied to the data. The measured inclusive single particle spectra and event shape distributions are presented in section 3.1 and are compared with corresponding data measured at the Z resonance and with some relevant Monte Carlo fragmentation models. Sections 3.2 and 3.3 present a phenomenological study of the energy dependence of the mean values and integrals over restricted ranges of event shape measures and a determination of α_s that is independent of fragmentation models. Finally, Section 4 summarizes the results.

2 Detector, Data and Data Analysis

The analysis is based on data taken with the DELPHI detector at energies between 130 and 136 GeV with an integrated luminosity of $5.9\,\mathrm{pb}^{-1}$.

DELPHI is a hermetic detector with a solenoidal magnetic field of 1.2 T. For this analysis only the tracking system and the electromagnetic calorimetry of DELPHI have been used.

The tracking detectors, which lie in front of the electromagnetic calorimeters, are a silicon micro-vertex detector VD, a combined jet/proportional chamber inner detector

ID, a time projection chamber TPC as the major tracking device, and the streamer tube detector OD in the barrel region; and the drift chamber detectors FCA and FCB in the forward region.

The electromagnetic calorimeters are the high density projection chamber HPC in the barrel, and the lead-glass calorimeter FEMC in the forward region. Detailed information about the construction and performance of DELPHI can be found in [9,10].

In order to select well-measured charged particle tracks and electromagnetic clusters, the cuts given in the upper part of Table 1 have been applied; they are similar to those for a related analysis at energies near the Z pole [11]. The cuts in the lower part of Table 1 have been used to select $e^+e^- \to Z/\gamma \to q\bar{q}$ events and suppress background processes such as two-photon interactions, beam-gas and beam-wall interactions, and leptonic final states. Furthermore they ensure a good experimental acceptance.

In contrast to the situation at the Z peak, hard initial state radiation (ISR) is important. In many cases the emitted photon reduces the centre of mass energy of the hadronic system to the Z mass. These events are often called "radiative return" events. The last two cuts in Table 1 are the most important in discarding them.

For the first of these two cuts, the event is clustered using the DURHAM algorithm [13] until only 2 jets remain. Assuming a single ISR photon emitted along the beam direction, the apparent γ energy is then calculated from the polar angles of these jets. Events are rejected if this energy, E_γ^{rec}, exceeds 20 GeV. Fig. 1 compares the reconstructed photon energy spectra in data and simulation (PYTHIA [14]). At $E_\gamma^{rec} \approx 40$ GeV, the enhancement due to radiative return events is clearly visible. The agreement between data and simulation is good.

For the second cut, each event is clustered (and forced) into three jets and rejected if any jet is dominated by electromagnetic energy. If an ISR event survives the first cut, one of the three jets is quite likely to be the single photon and thus to have a large fraction of electromagnetic energy.

This selection procedure has an efficiency of about 84% for events with no ISR ($E_\gamma \leq$ 1 GeV), and leads to a contamination below 16% from events with ISR above 20 GeV. A total of 321 events enter the further analysis. Two-photon events are strongly suppressed by the cuts shown in Table 1. They are estimated to be less than 0.3% of the selected sample, and have been neglected.

To correct for limited detector acceptance, limited resolution, and especially for the remaining influence of ISR, the spectra have been corrected using a bin by bin correction factor evaluated from a complete simulation of the DELPHI detector [10]. Events were generated using PYTHIA tuned to DELPHI data at Z energies [11]. In order to examine the corrections due to detector effects and due to ISR separately, the correction factor was split into two terms:

$$C = C_{det} \times C_{ISR} = \frac{h(f)_{gen,noISR}}{h(f)_{acc,noISR}} \times \frac{h(f)_{acc,noISR}}{h(f)_{acc}},$$

where $h(f)$ represents any normalized differential distribution as a function of an observable f. The subscripts "gen" and "acc" refer to the generated spectrum and that accepted after full simulation by the cuts described in Table 1, while "$noISR$" implies ISR photon energies below 1 GeV. The correction factors are shown in the upper insets in Figs. 2 - 4. The final correction factors are smooth as a function of the observables and are near unity in all cases. Note, however, that in many cases the detector and ISR corrections compensate each other.

Track selection	$0.2 \text{ GeV} \leq p \leq 100 \text{ GeV}$ $\Delta p/p \leq 1.3$ measured track length ≥ 30 cm $160^\circ \geq \theta \geq 20^\circ$ distance to I.P in $r\phi$ plane ≤ 4 cm distance to I.P. in $z \leq 10$ cm
E.M.Cluster	$0.5 \text{ GeV} \leq E \leq 100 \text{ GeV}$
Event selection	$N_{charged} \geq 7$ $150^\circ \geq \theta_{Thrust} \geq 30^\circ$ $E_{ch.}^{Jet1,2} \geq 10$ GeV $E_{ch.}^{Jet1} + E_{ch.}^{Jet2} \geq 40$ GeV $E_{\gamma}^{rec} \leq 20$ GeV $E_{E.M.}^{jet}/E^{jet} \leq 0.95$

Table 1: Selection of tracks, electromagnetic clusters, and events. Here p is the momentum, θ is the polar angle with respect to the beam (likewise θ_{Thrust} for the thrust axis), r is the radial distance to the beam-axis, z is the distance to the beam interaction point (I.P.) along the beam-axis, ϕ is the azimuthal angle; E is the electromagnetic cluster energy; $N_{charged}$ is the number of charged particles, $E_{ch.}^{Jet1,2}$ are the energies carried by charged particles in the two highest energy jets when clustering the event to three jets, E_{γ}^{rec} is the reconstructed ISR photon energy, and $E_{E.M.}^{jet}/E^{jet}$ is the highest fraction of electromagnetic energy in any of the three jets clustered.

To calculate the means and integrals of the event shape variables, the correction factors for the corresponding distributions were smoothed using polynomials and applied as a weight, event by event.

Corrections for ISR have been calculated using both PYTHIA and DYMU3 [15] and are similar. The total systematic error, originating from the fit, the generator, and the cut uncertainties, is small with respect to the statistical error for all distributions and bins, and has therefore been neglected.

3 Results

3.1 Inclusive and Shape Distributions and Model Comparisons

Fig. 2 shows corrected inclusive charged particle distributions as a function of $\xi_p = \ln 1/x_p$ where x_p is the scaled momentum $2p/\sqrt{s}$, the rapidity y_S with respect to the sphericity axis, and the momentum components transverse to the thrust axis in and out of the event plane, p_t^{in} and p_t^{out} respectively. The exact definitions of these variables and of the event shape variables used below are comprehensively collected in Appendix A of ref. [11]. Computer-readable files of the data distributions presented in this paper will be made available on the HEPDATA database [12].

In each case, the central plot compares the measured distribution at an average energy of 133 GeV with the predictions of the JETSET 7.4 [14], ARIADNE 4.08† [16], and HERWIG 5.8 [17] parton shower models. For completeness, the corresponding distribution measured at the Z [11] is shown compared to ARIADNE, which was found [11] to describe these data best. The models describe both the Z data and the high energy data well.

A skewed Gaussian [18] was used to fit the maximum of the ξ_p distribution (Fig. 2a). It is measured to be $\xi^* = 3.83 \pm 0.05$. This corresponds to a shift of 0.16 ± 0.05 with respect to the Z data ($\xi^*(M_Z) = 3.67 \pm 0.01$, [19]), to be compared with the change predicted by the MLLA (Modified Leading Log Approximation) [20,21] of:

$$\Delta\xi^* \approx \frac{1}{2} \cdot \ln \frac{E_{cm}}{M_Z} = 0.19 \ .$$

Given the small statistics of the high energy data, no conclusions are possible about the presence of scaling violation at high momenta, i.e. small ξ_p.

The rapidity distribution (Fig. 2b) shows the expected increase in multiplicity with centre-of-mass energy. The maximum rapidity is given by:

$$y_{max} \approx \frac{1}{2} \ln \left(\frac{E_{cm}}{2m_{hadron}} \right)^2 ,$$

leading to a shift of the upper "edge" of the rapidity plateau of ≈ 0.4. It can be seen that this expectation is fulfilled in the data.

Large changes are observed in the transverse momentum distributions (Figs. 2c,d). The cross-sections in the tails of the p_t^{in} and p_t^{out} distributions increase by factors of about 3 and 2 respectively. This is due to the larger available phase space for hard gluon emission at the higher energy.

It was checked that integrating over the rapidity and the p_t distributions yields an average total charged multiplicity value consistent with recent measurements from the LEP collaborations [22–25].

The lower insets in Fig. 2 show the observed and predicted ratios of the 133 GeV data to the Z data. This ratio is perfectly predicted by all models. This is true even in the case of the p_t^{out} distribution, which is imperfectly described by the models at the Z. This failure of the p_t^{out} description presumably comes from the missing higher order terms in the Leading Log Approximation [11,26], which is basic to all parton shower models. If so, it is not expected to appear in the evolution with energy.

Fig. 3 presents the distributions as a function of 1−Thrust $(1-T)$, Major (M), Minor (m), and Oblateness (O). Most obvious is the trend to populate small values of $1-T$, M and m, and correspondingly to depopulate higher values, at the higher energy. Thus the events appear more 2-jet-like on average. The Minor distribution in lowest order depends quadratically on α_s, which explains why the depopulation appears most clearly for this variable. For similar reasons, this is also observed for the hemisphere Broadenings B_{max}, B_{min}, B_{sum} and B_{diff} (Fig. 4). Again the behaviour observed in the data is reproduced very well by the models.

Fig. 5 shows the 2-jet, 3-jet, 4-jet and 5-jet rates, R_2, R_3, R_4 and R_5, using both the JADE [27] and DURHAM [13] algorithms, as a function of y_{cut}. The high energy data agree well with the generator predictions tuned to Z data. In particular, there is no significant excess of multijet events in the data.

†ARIADNE simulates only the parton shower process and employs the JETSET routines to model the hadronization and decays.

3.2 Energy Dependence of Event Shapes and Investigation of Leading Power Corrections

Several sources are expected to lead to an energy dependence of event shape distributions [3,4]:

- the logarithmic dependence of the strong coupling constant, α_s,
- the hadronization process, leading to a dependence proportional to $1/E_{cm}$,
- renormalons, which are connected to the divergence of perturbation theory at high orders and lead to power suppressed terms proportional to $1/E_{cm}^p$, $p \geq 1$ [6].

In order to study these contributions, the means of the event shape distributions, their integrals over restricted ranges (denoted by $\int f$) chosen to exclude the 2-jet region, and the 3-jet rates measured at Z energies and at 133 GeV, are compared where possible with the data of other experiments, mainly at lower energies [28]. The measured values are given in Table 2.

Observable		$E_{cm} = 91.2$ GeV	$E_{cm} = 133$ GeV
$\langle 1-T \rangle$		0.0678 ± 0.0002	0.0616 ± 0.0034
$\left\langle \frac{M_h^2}{E_{vis}^2} \right\rangle$		0.0533 ± 0.0001	0.0506 ± 0.0030
$\left\langle \frac{M_d^2}{E_{vis}^2} \right\rangle$		0.0331 ± 0.0001	0.0337 ± 0.0026
$\langle B_{sum} \rangle$		0.1144 ± 0.0003	0.1050 ± 0.0036
$\langle B_{max} \rangle$		0.0767 ± 0.0002	0.0730 ± 0.0037
$\int (1-T)$	$T < 0.8$	0.0130 ± 0.0005	—
$\int \frac{M_h^2}{E_{vis}^2}$	$\frac{M_h^2}{E_{vis}^2} > 0.1$	0.0209 ± 0.0005	—
$\int$ EEC	$\lvert\cos\theta\rvert < 0.5$	0.0939 ± 0.0011	0.094 ± 0.010
$\int B_{sum}$	$B_{sum} > 0.2$	0.0218 ± 0.0002	—
$\int B_{max}$	$B_{max} > 0.1$	0.0355 ± 0.0001	—
R_3^{Jade}	$(y_{cut} = 0.08)$	0.1821 ± 0.0007	0.182 ± 0.024
R_3^{Durham}	$(y_{cut} = 0.04)$	0.1449 ± 0.0006	0.142 ± 0.021

Table 2: Event shape means, integrals, and 3-jet event rates at the Z and at 133 GeV. The ranges of the integrals are restricted in order to largely exclude the contribution of 2-jet events. There are too few events to calculate them at 133 GeV, except in the EEC case.

Fig. 6 compares the energy dependence of several of these observables with the predictions of the ARIADNE, HERWIG, and JETSET parton shower models. The models, which have been tuned to DELPHI data taken at Z energies [11], agree very well with the experimental data over the whole energy range. Thus the models seem to account correctly for the different sources of energy dependence quoted above. Some discrepancies between the models are visible at lower energies. At higher energies, the agreement is good.

The model predictions at the "parton level", i.e. before hadronisation, are shown as well. The difference between the "hadron level" and "parton level" predictions indicates the size of the so called "hadronisation correction" applied in most α_s analyses of event shape distributions. The model dependence of this difference can be taken as a measure of the uncertainty of this correction. The influence of the hadronisation is strongest for the integral of the energy-energy correlation $\int$EEC, and for $\langle 1-T\rangle$ and $\langle B_{sum}\rangle$. The correction is smaller for the wide hemisphere broadening $\langle B_{max}\rangle$ and the heavy hemisphere mass $\langle M_h^2/E_{vis}^2\rangle$. This is expected, since the low mass side of an event enters in $\int$EEC, $\langle 1-T\rangle$ and $\langle B_{sum}\rangle$, but does not appear in the calculation of $\langle M_h^2/E_{vis}^2\rangle$ and $\langle B_{max}\rangle$. For the difference of hemisphere masses, $\langle M_d^2/E_{vis}^2\rangle$, as expected, the hadronisation effects largely cancel: the parton level expectation is above the hadron level one for this observable. The jet rates R_3^{Jade} and R_3^{Durham} show a more complex behaviour: the hadronisation correction first falls rapidly with increasing energy; then at medium energies it changes sign; and finally it becomes very small ($\leq$5% for all models) at the highest energies displayed.

Figure 7 shows integrals of the $(1-T)$, M_h^2/E_{vis}^2, B_{sum} and B_{max} distributions over the restricted ranges of the variables chosen to largely exclude 2-jet events (see Table 2). At the hadron level, the models describe the data well. The differences between the hadron level predictions and the corresponding parton level predictions vanish much faster (approximately like $1/E_{cm}^2$) than for the corresponding mean values. This is different from the behaviour of the $\int$EEC data in Fig. 6 (for which 2 jet events are also largely excluded): the slower fall-off of the hadronisation correction is preserved in the case of this variable. This behaviour of $\int$EEC has been predicted in [6].

The comparisons of the models with the energy dependence of the shape observables suggest that the variables M_h^2/E_{vis}^2, B_{max}, and the jet rates can be calculated most reliably, because the hadronisation corrections are particularly small for these variables at high energy.

In order to assess the sizes of the individual contributions, the energy dependence of each event shape mean for which lower energy data are available was fitted by :

$$\langle f\rangle = \frac{1}{\sigma_{tot}}\int f\frac{d\sigma}{df}df = \langle f_{pert}\rangle + \langle f_{pow}\rangle \ , \tag{1}$$

and similarly for each restricted-range integral, where

- f_{pert} is the $\mathcal{O}(\alpha_s^2)$ expression for the event shape distribution:

$$\langle f_{pert}\rangle \ = \ \frac{\alpha_s(\mu)}{2\pi}\cdot A\left(1-\frac{\alpha_s(E_{cm})}{\pi}\right)+\left(\frac{\alpha_s(\mu)}{2\pi}\right)^2\cdot\left(A\cdot 2\pi b_0\cdot\log\frac{\mu^2}{E_{cm}}+B\right) \tag{2}$$

  where A and B are parameters available from theory [1], $b_0=(33-2N_f)/12\pi$, and μ is the renormalisation scale,
- f_{pow} is a simplified power dependence with free parameters C_1 and C_2 to account for the fragmentation plus renormalon dependence:

$$\langle f_{pow}\rangle = \frac{C_1}{E_{cm}}+\frac{C_2}{E_{cm}^2}. \tag{3}$$

The results of these fits are presented in Table 3 and compared with the data in Fig. 8.

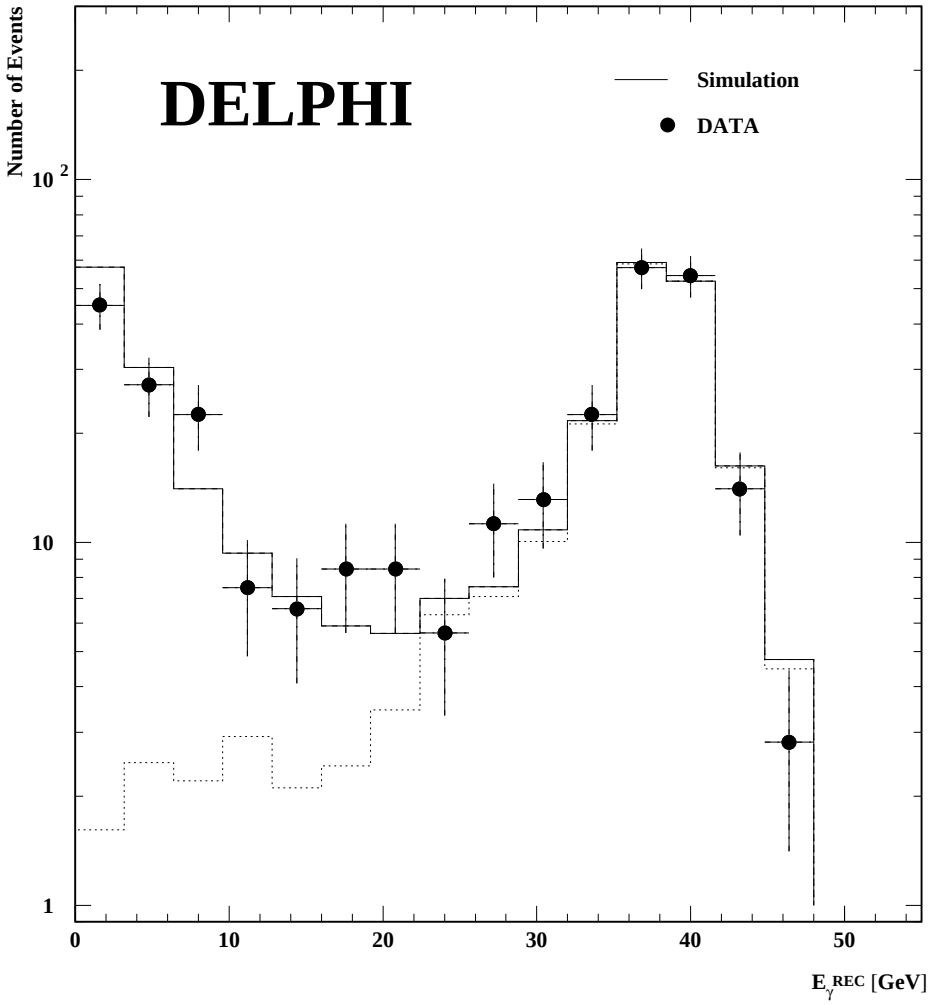

Figure 1: Reconstructed energy spectrum of photons from initial state radiation (ISR). The peak at E_γ^{rec} near 40 GeV due to radiative return to the Z is clearly seen. Events with E_γ^{rec} above 20 GeV are rejected in this analysis. The dotted histogram shows the E_γ^{rec} distribution for fully simulated events generated with $E_\gamma \geq 20$ GeV.

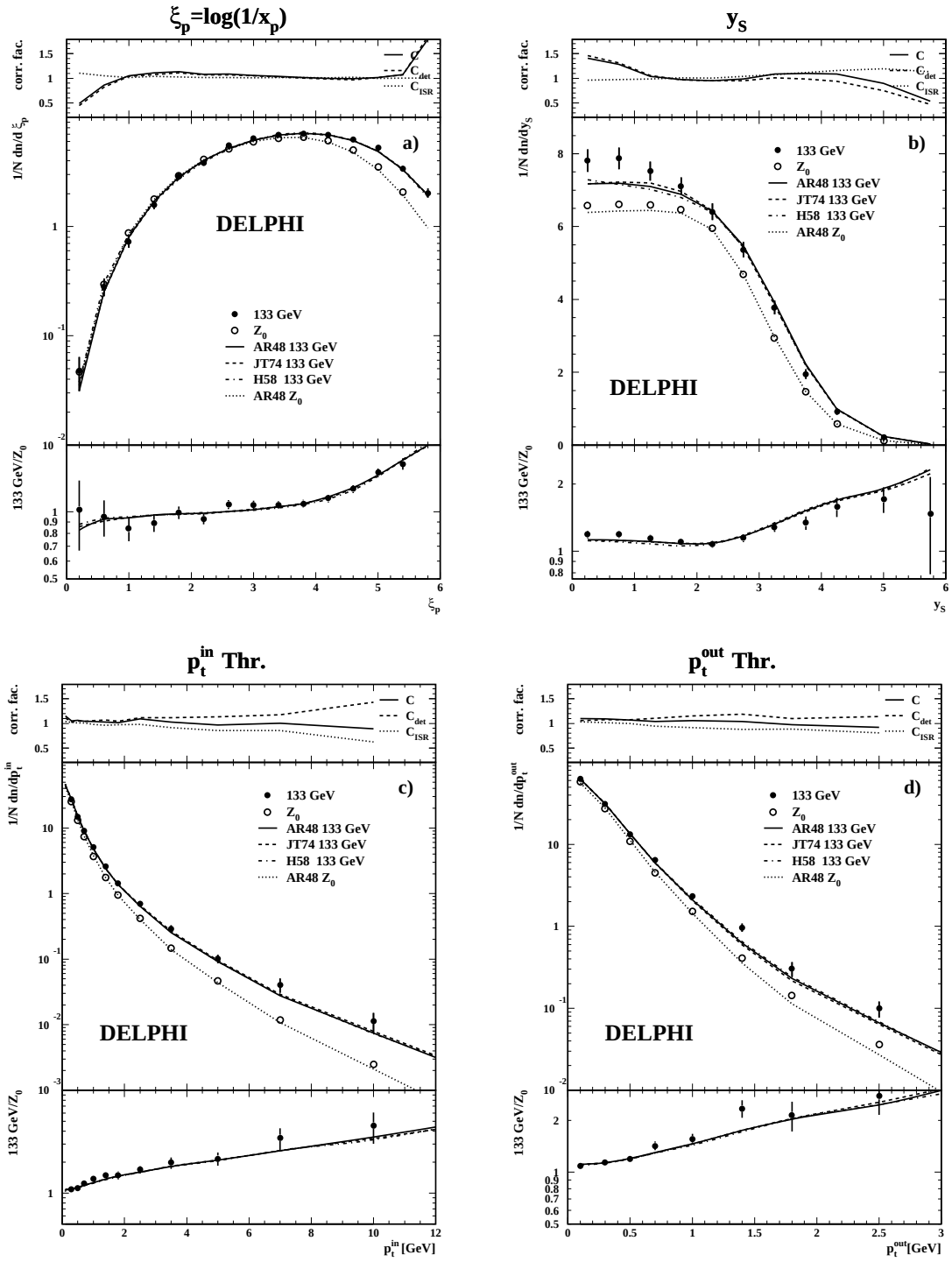

Figure 2: The four central plots show inclusive charged particle distributions at 133 GeV (full circles) and at the Z (open circles) as a function of (a) ξ_p, (b) y_S, (c) p_t^{in}, and (d) p_t^{out}. The curves show the predictions from ARIADNE 4.8 (full curve for 133 GeV, dotted for the Z) and, for 133 GeV only, from JETSET 7.4 (dashed) and HERWIG 5.8 (dot-dashed). The upper insets display the correction factors explained in the text: the dashed line shows the detector correction, the dotted line the ISR correction, and the full line the total correction. The lower insets show the ratio of the 133 GeV data to the Z data and the corresponding model predictions.

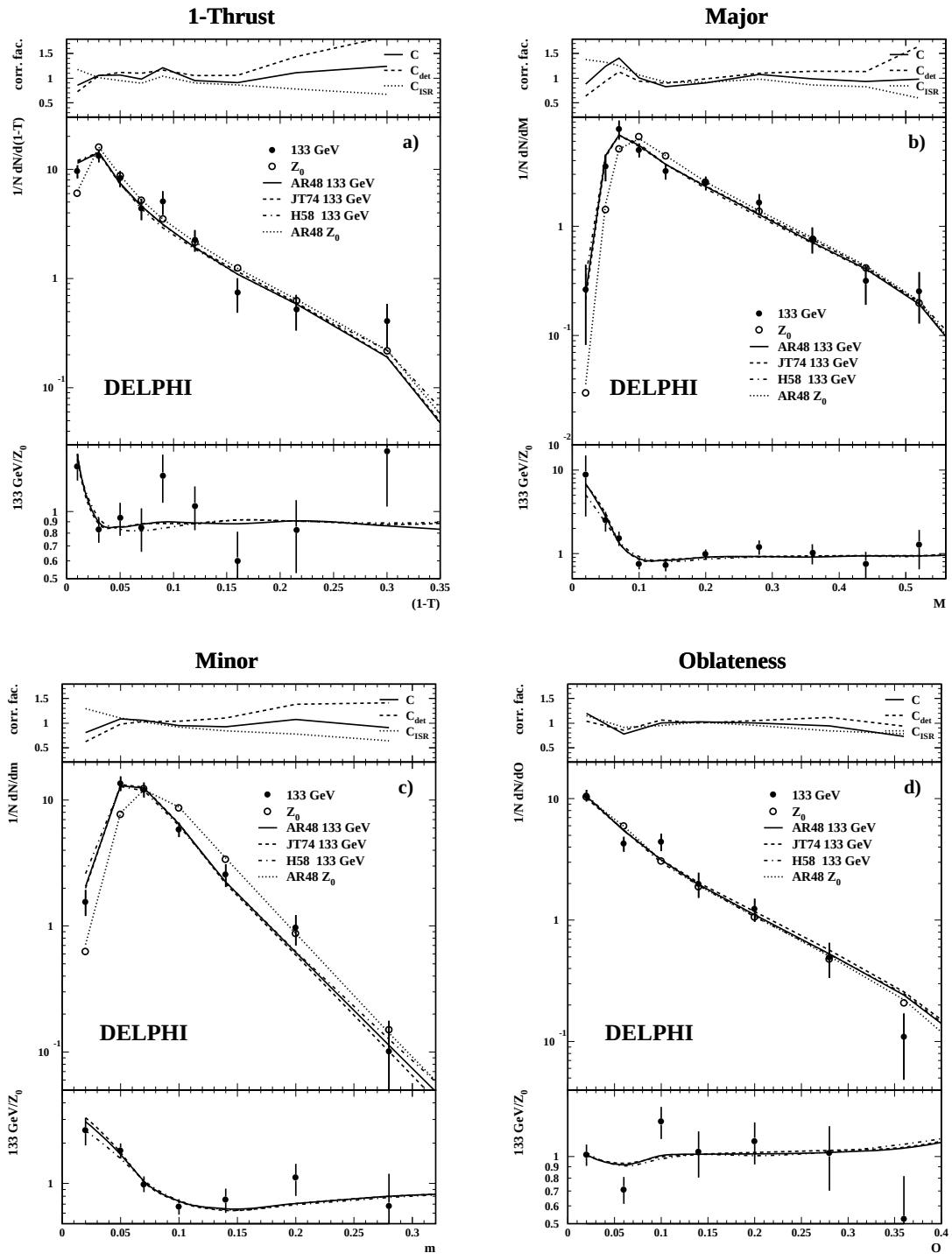

Figure 3: (*a*) 1-Thrust, (*b*) Major, (*c*) Minor and (*d*) Oblateness distributions. The insets, symbols and curves are as in Fig. 2.

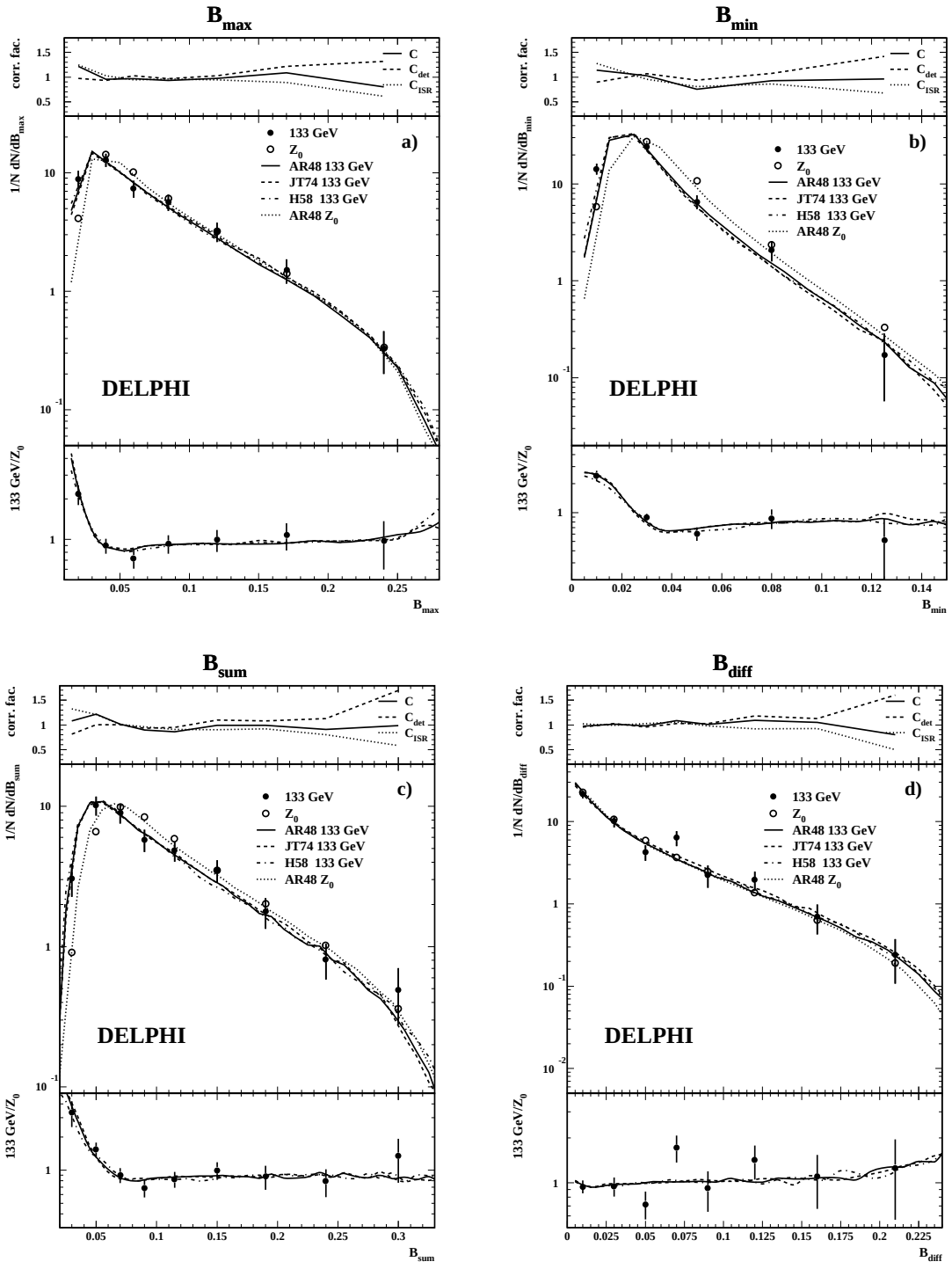

Figure 4: Distribution of (a) Wide Hemisphere Broadening, (b) Narrow Hemisphere Broadening, (c) Total Hemisphere Broadening and (d) Difference of the Hemisphere Broadenings. The insets, symbols and curves are as in Fig. 2.

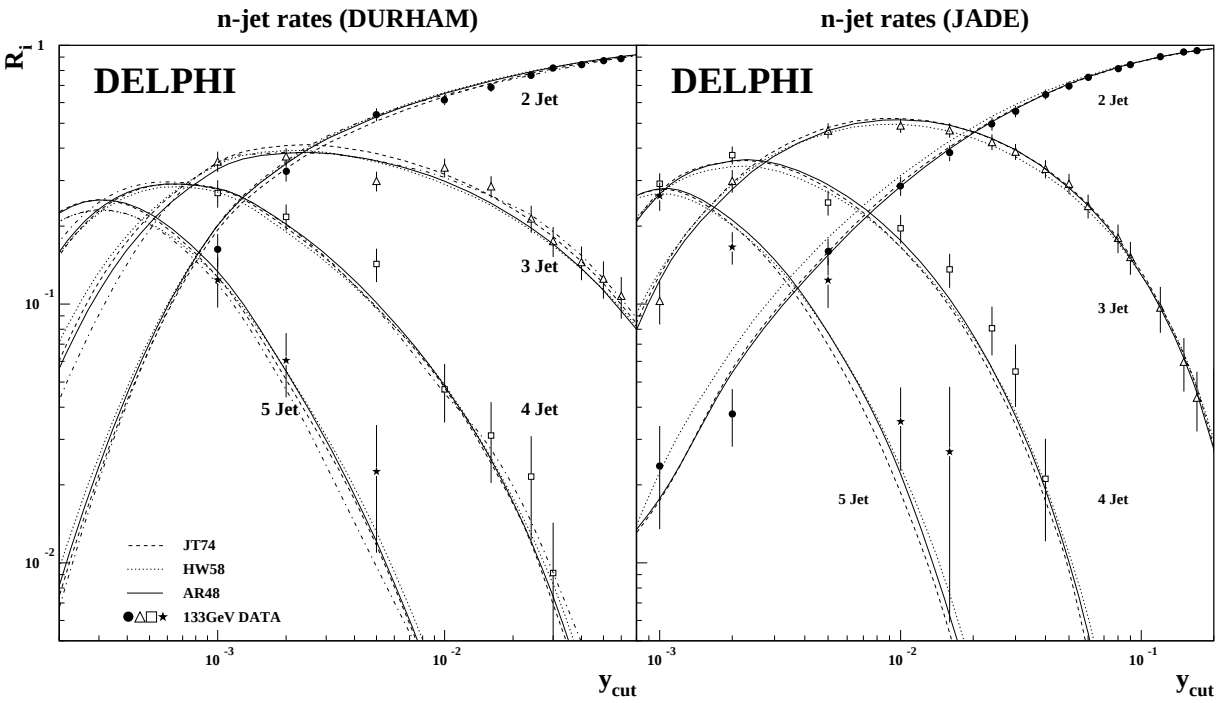

Figure 5: Measured 2-jet, 3-jet, 4-jet and 5-jet rates at 133 GeV as a function of y_{cut} for the Durham and JADE jet algorithms compared with the predictions of ARIADNE 4.8 (full curve), JETSET 7.4 (dashed), and HERWIG 5.8 (dotted).

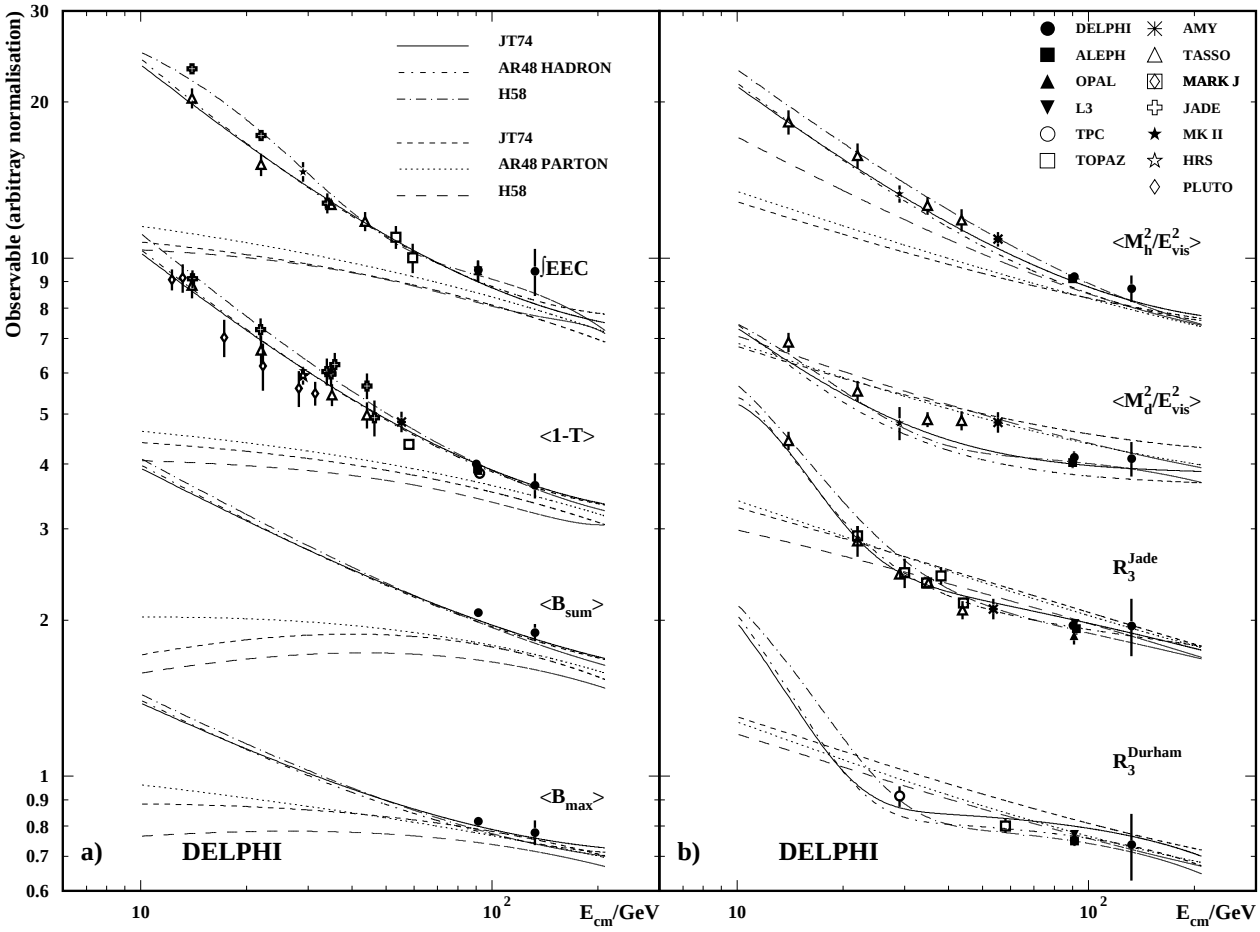

Figure 6: Energy dependence of event shape variables using the cuts (where relevant) defined in Table 2 compared with predictions of the ARIADNE, HERWIG, and JETSET fragmentation models. The curves correspond to the hadronic (full and dot-dashed curves close to data) and partonic (dashed curves showing weaker energy dependence) final states.

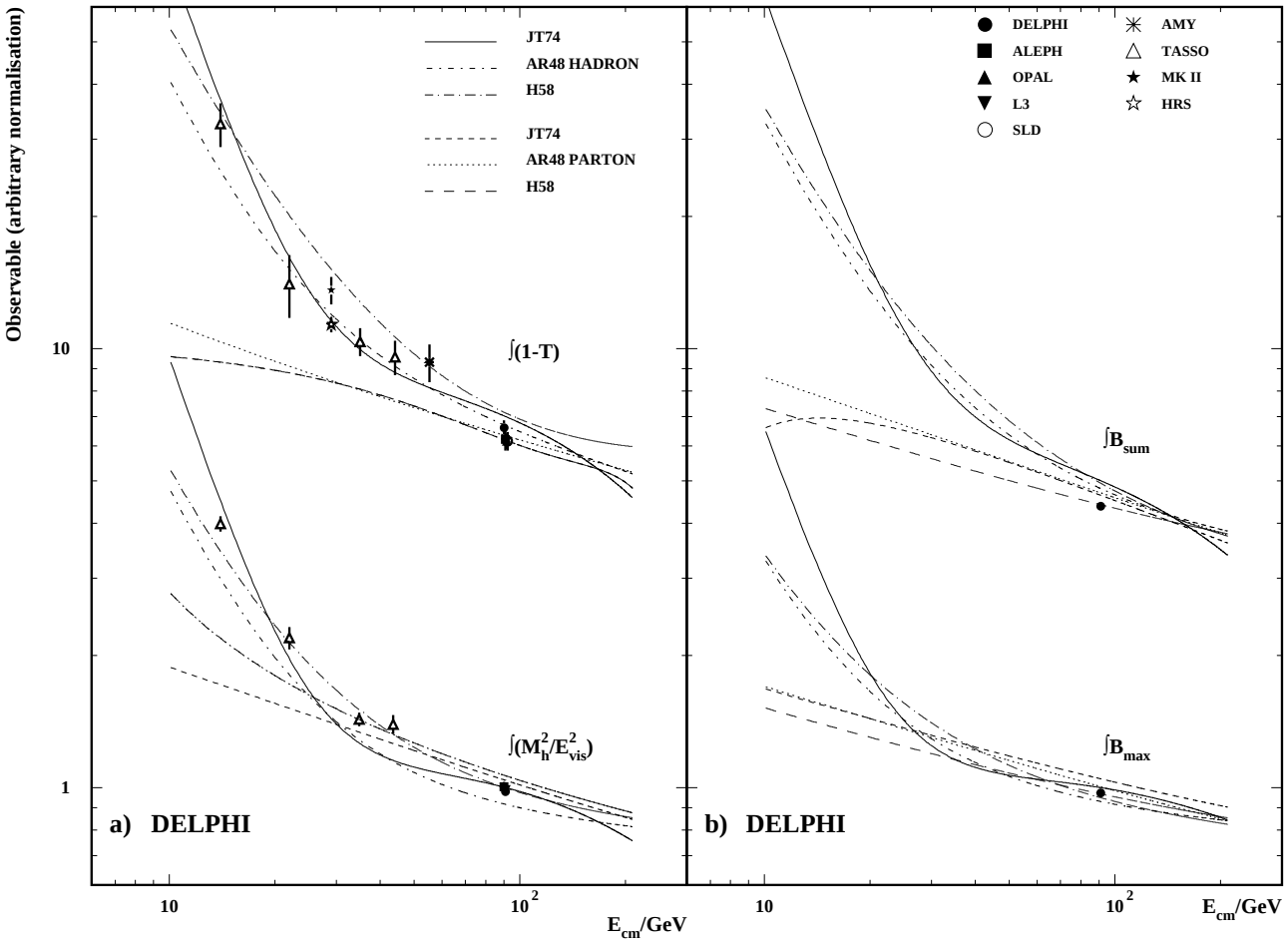

Figure 7: Energy dependence of event shape variables using the cuts (where relevant) defined in Table 2 compared with predictions of the ARIADNE, HERWIG, and JETSET fragmentation models. The curves correspond to the hadronic (full and dot-dashed curves close to data) and partonic (dashed curves showing weaker energy dependence) final states.

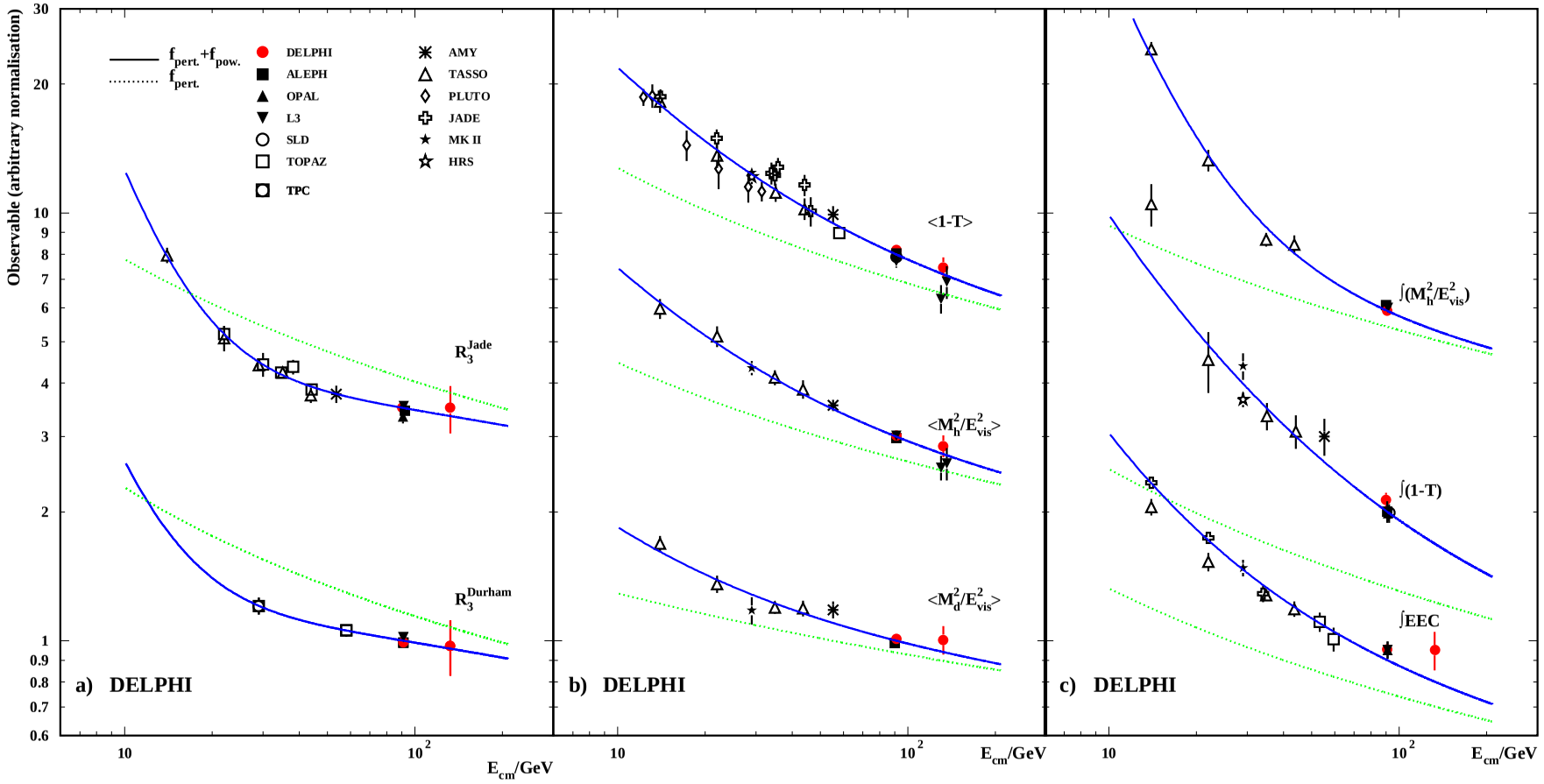

Figure 8: Energy dependence of event shape observables using the cuts defined in Table 2. The curves are results of the fits to equations (1-3). The corresponding parameters are given in Table 3. In b) the fits with $C_2 = 0$ are displayed. The dotted lines correspond to the pure second order perturbative prediction, $\langle f_{pert} \rangle$, the full curves represent the sum of the perturbative and power terms, $\langle f_{pert} \rangle + \langle f_{pow} \rangle$.

Observable	C_1(GeV)	C_2(GeV^2)	$\alpha_s(M_Z)$	χ^2/ndf
R_3^{Jade} $(y_{cut}=0.08)$	-3.59 ± 0.55	61.3 ± 7.6	0.123 ± 0.002	8.0/13
R_3^{Durham} $(y_{cut}=0.04)$	-2.53 ± 3.15	31.0 ± 28.4	0.137 ± 0.019	1.8/3
$\langle 1-T \rangle$	0.67 ± 0.20	1.0 ± 2.0	0.126 ± 0.004	43.8/26
	0.77 ± 0.07	0.0 (fixed)	0.125 ± 0.002	44.1/27
$\left\langle \frac{M_h^2}{E_{vis}^2} \right\rangle$	0.76 ± 0.26	-2.9 ± 3.3	0.116 ± 0.006	6.3/9
	0.54 ± 0.08	0.0 (fixed)	0.121 ± 0.002	7.1/10
$\left\langle \frac{M_d^2}{E_{vis}^2} \right\rangle$	0.03 ± 0.15	2.0 ± 1.8	0.100 ± 0.006	5.6/6
	0.0 (fixed)	2.4 ± 0.5	0.101 ± 0.002	5.7/7
	0.19 ± 0.04	0.0 (fixed)	0.094 ± 0.002	6.9/7
$\int(1-T)$ $T < 0.8$	0.36 ± 0.03	0.9 ± 1.18	0.120 (fixed)	19.2/9
$\int \frac{M_h^2}{E_{vis}^2}$ $\frac{M_h^2}{E_{vis}^2} > 0.1$	0.05 ± 0.03	9.6 ± 0.9	0.120 (fixed)	7.1/5
$\int$ EEC $\lvert\cos\theta\rvert < 0.5$	1.26 ± 0.05	4.6 ± 0.8	0.120 (fixed)	66/12

Table 3: Fits to the mean values and integrals of event shape variables at all available energies.

Satisfactory fits are obtained in most cases. Only for $\langle 1-T \rangle$, $\int(1-T)$, and especially for $\int$ EEC are the χ^2/ndf values too large. However, Fig. 8 shows that this is largely due to discrepancies between the data of the different experiments.

It is remarkable that this simple model leads to perturbative and hadronisation contributions comparable with those obtained from the fragmentation models (compare Fig. 8 with Figs. 6 and 7). The values of α_s obtained are reasonable for many fits. However they should not be interpreted quantitatively, given the simplied power dependence assumed in the fits.

The fit for R_3^{Jade} requires terms proportional to $1/E$ and to $1/E^2$ as well as a significant $\mathcal{O}(\alpha_s)$ term (compare Table 3 and Fig. 8a). The term proportional to $1/E$ is negative and is partly compensated over a wide range in energy by a strong contribution proportional to $1/E^2$. Thus the overall power correction for R_3^{Jade} is small over a wide range in energy.

The same behaviour is perhaps observed for R_3^{Durham}, although the power terms are very poorly determined in this case because no very low energy data are available, and they could both be absent. This is unfortunate, since the Monte Carlo predictions suggest a similar energy behaviour for R_3^{Durham} and R_3^{Jade} (see Fig. 6), contrary to a theoretical prediction [29] which expects a $1/E$ term for R_3^{Jade} and only a $1/E^2$ power term in case of R_3^{Durham}.

The event shape means $\langle 1-T \rangle$ and $\langle M_h^2/E_{vis}^2 \rangle$ require only a $1/E$ power behaviour, as predicted in [7,29]: fixing C_2 to zero changes χ^2 only marginally (see Table 3). For $\langle M_d^2/E_{vis}^2 \rangle$, the overall power correction is smaller, and successful fits can be obtained using either the $1/E$ or $1/E^2$ term alone. In all cases, however, the fitted value of α_s is rather small. For $\langle M_d^2/E_{vis}^2 \rangle$, contrary to other observables, the f_{pert} term determined from the fit (see Fig. 8b) and the parton level curves (see Fig. 6b) are on opposite sides of the data.

$E_{cm} \leq M_Z$				
Observable	$\bar{\alpha}_0$	$\alpha_s(M_Z)$	$\Lambda_{\overline{MS}}$[MeV]	χ^2/ndf
$\langle 1-T \rangle$	0.534 ± 0.012	0.118 ± 0.002	224 ± 19	43/24
$\langle M_h^2/E_{vis}^2 \rangle$	0.435 ± 0.015	0.114 ± 0.002	182 ± 18	4.1/7

Table 4: Results of the fits to the energy dependence of the event shape means according to the prescription given in [7]. The errors shown are experimental.

It is of interest to search for observables which have no leading $1/E$ term, so that the power correction disappears more rapidly with increasing energy, and the α_s value extracted at high energy may be more reliable. Fig. 8c shows the fits to $\int (M_h^2/E_{vis}^2)$, $\int (1-T)$ and $\int$ EEC, where the ranges of the variables dominated by 2 jet events are excluded in all cases. As the data quality for these variables is relatively poor, α_s was fixed to 0.120 for these fits. It is indeed possible to describe the energy dependence of $\int (M_h^2/E_{vis}^2)$ by a $1/E^2$ power term only, but $\int (1-T)$ and $\int$ EEC both require significant $1/E$ terms. It was correctly predicted [6] that the leading power term of $\int (M_h^2/E_{vis}^2)$ should be proportional to $1/E^2$, whereas for $\int$ EEC it should be proportional to $1/E$, because 2-jet events can be shown to always contribute to $\int$ EEC while only events where a hard gluon radiation took place enter $\int (M_h^2/E_{vis}^2)$. However, the same argument was used to predict that, as for $\int (M_h^2/E_{vis}^2)$, the leading power term for $\int (1-T)$ should be proportional to $1/E^2$, and it is not. This may be because, for $\int (1-T)$, the properties of the whole event enter, whereas while for $\int (M_h^2/E_{vis}^2)$ only the hemisphere containing the hard radiation contributes.

It is also worth noting that Fig. 6b) suggests that $\int B_{max}$ may also show a power behaviour similar to that of $\int (M_h^2/E_{vis}^2)$ and thus be equally well suited for determining α_s.

3.3 Fragmentation Model Independent Determination of α_s

In order to infer α_s quantitatively from the 133 GeV data independently of fragmentation models, the observables $\langle 1-T \rangle$ and $\langle M_H^2/E_{vis}^2 \rangle$ were chosen as their power terms are well determined by the data and agree with expectations [7,29], and they are reasonably well measured at 133 GeV. The prescription given in [7] was followed, where $\langle f \rangle = \langle f_{pert} \rangle + \langle f_{pow} \rangle$ with

$$\langle f_{pow} \rangle = a_f \cdot \frac{\mu_I}{E_{cm}} \left[\bar{\alpha}_0(\mu_I) - \alpha_s(\mu) - \left(b_0 \cdot \log \frac{\mu^2}{\mu_I^2} + \frac{K}{2\pi} + 2b_0 \right) \cdot \alpha_s^2(\mu) \right], \qquad (4)$$

$\bar{\alpha}_0$ being a non-perturbative parameter accounting for the contributions to the event shape below an infrared matching scale μ_I, $K = (67/18 - \pi^2/6)C_A - 5N_f/9$ and $a_f = 4C_f/\pi$. Using this approach the value of α_s was inferred in two steps.

Firstly, equations 1, 2 and 4 were used to fit α_s and $\bar{\alpha}_0$ to the variables $\langle 1-T \rangle$ and $\langle M_h^2/E_{vis}^2 \rangle$ obtained from data for energies up to $E_{cm} = M_Z$ [11,28] using $\mu_I = 2$ GeV and $\mu = E_{cm}$. The results of these fits are listed in Table 4. The value of $\bar{\alpha}_0$ should be around 0.5 [29], in agreement with the observation. To estimate the influence of higher order terms missing in the second order prediction, the renormalisation scale μ in equation 4 was varied between $0.5E_{cm}$ and $2E_{cm}$. This changed α_s by $^{+0.005}_{-0.004}$. The scale μ_I was varied by ± 1 GeV, ie by $\pm 50\%$, which changed $\alpha_s(M_Z)$ by ± 0.002. Thus, the combined value

DELPHI $\langle E_{cm} \rangle = 133$ GeV				
Observable	$\bar{\alpha}_0$ (fixed)	$\alpha_s(M_Z)$	$\Lambda_{\overline{MS}}$[MeV]	$\alpha_s(133$ GeV)
$\langle 1-T \rangle$	0.534	0.124 ± 0.008	316^{+135}_{-106}	0.117 ± 0.007
$\langle M_h^2/E_{vis}^2 \rangle$	0.435	0.122 ± 0.009	276^{+151}_{-110}	0.115 ± 0.008

Table 5: Results from the evaluation of α_s from 133 GeV data using equation 4. The errors shown are experimental.

of α_s and $\Lambda_{\overline{MS}}$ from the data up to and including Z energies [11,28] is:

$$\alpha_s(M_Z) = 0.116 \pm 0.002_{exp}{}^{+0.006}_{-0.005 theo} \quad \Lambda_{\overline{MS}} = (203 \pm 19_{exp}{}^{+75}_{-50 theo}) \text{ MeV}.$$

The result is consistent with other determinations of α_s from event shapes [3]. However, it should be noted that no Monte Carlo fragmentation model was needed for this measurement.

Secondly, values of α_s were obtained from the data at $\langle E_{cm} \rangle = 133$ GeV alone, using the values of $\bar{\alpha}_0$ extracted from the lower energy data. The results are listed in Table 5. To estimate the scale error, μ and μ_I were varied as above, using $\bar{\alpha}_0$ from the corresponding low energy data fit. The renormalisation scale error is $^{+0.005}_{-0.004}$, and the error from the choice of μ_I is ± 0.001. Combining the experimental errors assuming maximal correlation gives:

$$\alpha_s(133 \text{ GeV}) = 0.116 \pm 0.007_{exp}{}^{+0.005}_{-0.004 theo} \quad \Lambda_{\overline{MS}} = (296^{+135}_{-106 exp}{}^{+101}_{-\ 64 theo}) \text{ MeV},$$

consistent with the value at the Z mass. This is comparable with recent measurements of $\alpha_s(133$ GeV) from other LEP collaborations [23–25]. Even though the theoretical errors can be ignored when comparing $\alpha_s(M_Z)$ with $\alpha_s(133$ GeV), the small statistics of the high energy data so far do not allow a conclusion on the running of α_s between the Z energy and 133 GeV.

4 Summary

Inclusive charged particle distributions and event shape distributions have been measured from 321 events obtained with the DELPHI detector at centre of mass energies of 130 and 136 GeV.

Compared with the Z data, the ξ_p and rapidity distributions show the expected increases in the peak position and maximum rapidity respectively, a large increase in particle production is observed at high transverse momentum, and the events appear more 2-jet-like on average.

The ARIADNE, HERWIG, and JETSET fragmentation models quantitatively describe the changes observed in the inclusive charged particle spectra and in the event shape distributions.

The energy dependence of the event shape means is very well described by the models, as well as by a simple power law plus $\mathcal{O}(\alpha_s^2)$ dependence. The hadronisation corrections estimated by the two methods are similar. Among the observables considered, the hadronisation correction at high energy is smallest ($\leq$5%) for the jet rates, for the heavy hemisphere mass variable $\langle M_h^2/E_{vis}^2 \rangle$, and for the wide hemisphere broadening $\langle B_{max} \rangle$.

From the energy dependences of the mean (1−Thrust) and heavy hemisphere mass, α_s is measured to be:

$$\alpha_s(M_Z) = 0.116 \pm 0.002_{exp}{}^{+0.006}_{-0.005}{}_{theo}$$

from the data up to Z energies [28] and

$$\alpha_s(133\ \mathrm{GeV}) = 0.116 \pm 0.007_{exp}{}^{+0.005}_{-0.004}{}_{theo}$$

from the high energy data reported here, independently of Monte Carlo fragmentation model corrections.

The smaller theoretical uncertainty of $\alpha_s(133\ \mathrm{GeV})$ results from from the higher energy, and the improved convergence of the perturbation series due to the inclusion of equation 4 compared to an ansatz using only f_{pert}. However, the large statistical error of α_s compared to [23–25] results from the almost linear relation between $\langle f \rangle$ and α_s.

No conclusion is possible on a running of the strong coupling constant between the Z energies and 133 GeV because of the small statistics of the high energy data.

Acknowledgements

We are greatly indebted to our technical collaborators and to the funding agencies for their support in building and operating the DELPHI detector, and to the members of the CERN-SL Division for the excellent performance of the LEP collider.

References

[1] Z Physics at LEP I, CERN 89–08 Vol. 1.
[2] R.K. Ellis, D.A. Ross, A.E. Terrano, Nucl. Phys. **B178** (1981) 421.
[3] B.R. Webber, Proceedings of the XXVII ICHEP Glasgow 1994, Vol 1.
[4] PLUTO Coll., C. Berger et al., Z. Phys. **C12** (1982) 297.
[5] B.R. Webber, Phys. Lett. **B339** (1994) 148.
[6] P. Nason and M.H. Seymour, Nucl. Phys. **B454** (1995) 291.
[7] Yu.L. Dokshitzer and B.R. Webber, Phys. Lett. **B352** (1995) 451.
[8] R. Akhoury, V.I. Zakharow, Nucl. Phys. **B465** (1996) 295.
[9] DELPHI Coll., P. Aarnio et al., Nucl. Instr. Meth. **A303** (1991) 187.
[10] DELPHI Coll., P. Abreu et al., Nucl. Instr. Meth. **A378** (1996) 57.
[11] DELPHI Coll., P. Abreu et al., CERN–PPE/96–120 subm. to Z. Phys. **C**.
[12] HEPDATA Database, http://durpdg.dur.ac.uk/HEPDATA/REAC, search command "EXP CERN-LEP-DELPHI";
see also "HEPDATA - World Wide Web User Guide", M.R. Whalley, DPDG/96/01.
[13] S. Catani et al., Phys. Lett. **B269** (1991) 432.
[14] T. Sjöstrand, Comp. Phys. Comm. **39** (1986) 347;
T. Sjöstrand and M. Bengtsson, Comp. Phys. Comm. **46** (1987) 367.
[15] J.E. Campagne and R. Zitoun, Z. Phys. **C43** (1989) 469.
[16] L. Lönnblad, Comp. Phys. Comm. **71** (1992) 15.
[17] G. Marchesini et al., Comp. Phys. Comm. **67** (1992) 465.
[18] C.P. Fong and B.R. Webber, Phys. Lett. **B229** (1989) 289.
[19] DELPHI Coll., P. Abreu et al., Phys. Lett. **B275** (1992) 231.
[20] Yu.L. Dokshitzer et al., Basics of Perturbative QCD,
Editions Frontières, Gif-sur-Yvette, 1991.
[21] M. Schmelling, Physica Scripta **51** (1995) 676.
[22] DELPHI Coll., P. Abreu et al., Phys. Lett. **B372** (1996) 172.
[23] L3 Coll., M. Acciarri et al., Phys. Lett. **B371** (1996) 137.
[24] ALEPH Coll., CERN–PPE/96–43, to be published in Phys. Lett. **B**.
[25] OPAL Coll., CERN–PPE/96–47, to be published in Phys. Lett. **B**.
[26] Physics at LEP II, CERN 96-01 Vol. 2, I. G. Knowles et al.,
QCD Event Generators, hep-ph/9601212.
[27] S. Bethke et al., Phys. Lett. **B213** (1988) 235.
[28] ALEPH Coll., D. Decamp et al., Phys. Lett. **B284** (1992) 163.
ALEPH Coll., D. Buskulic et al. Z. Phys. **C55** (1992) 209.
AMY Coll., I.H. Park et al., Phys. Rev. Lett. **62** (1989) 1713.
AMY Coll., Y.K. Li et al. Phys. Rev. **D41** (1990) 2675.
CELLO Coll., H.J. Behrend et al., Z. Phys. **C44** (1989) 63.
HRS Coll., D. Bender et al., Phys. Rev. **D31** (1985) 1.
JADE Coll., W. Bartel et al., Z. Phys. **C25** (1984) 231.
JADE Coll., W. Bartel et al., Z. Phys. **C33** (1986) 23.
L3 Coll., B. Adeva et al. Z. Phys. **C55** (1992) 39.
Mark II Coll., A. Peterson et al., Phys. Rev. **D37** (1988) 1.
Mark II Coll., S. Bethke et al., Z. Phys. **C43** (1989) 325.
MARK J Coll., D. P. Barber et al., Phys. Rev. Lett. **43** (1979) 831.
OPAL Coll., P. Acton et al., Z. Phys. **C59** (1993) 1.
PLUTO Coll., C. Berger et al., Z. Phys. **C12** (1982) 297.
SLD Coll., K. Abe et al. Phys. Rev. **D51** (1995) 962.

TASSO Coll., W. Braunschweig et al., Phys. Lett. **B214** (1988) 293.
TASSO Coll., W. Braunschweig et al., Z. Phys. **C45** (1989) 11.
TASSO Coll., W. Braunschweig et al., Z. Phys. **C47** (1990) 187.
TOPAZ Coll., I. Adachi et al., Phys. Lett. **B227** (1989) 495.
TOPAZ Coll., K. Nagai et al., Phys. Lett. **B278** (1992) 506.
TOPAZ Coll., Y. Ohnishi et al., Phys. Lett. **B313** (1993) 475.
TPC/2γ Coll., D.A. Bauer et al., LBL–35812, SLAC-PUB-6518 (1994).
[29] B.R. Webber, "Hadronic Final States", talk given at Workshop on DIS and QCD in Paris, April 1995, Cavendish-HEP-95/11, hep-ph/9510283.